A Nondestructive Method for Determining Weathering and Consolidation of Stone

Zhong Shihang and Huang Kezhong

Natural weathering poses the greatest threat to exposed ancient stone statues, many of which are fine works of art. One method of preventing weathering is to treat the surface with a chemical consolidant. The consolidant should penetrate the surface and harden, thereby reinforcing it and increasing its strength and weathering resistance. The consolidant must satisfy the following conditions: (1) it must not change the appearance and color of the statue; (2) it must be able to penetrate the stone deeply enough so that the surface does not exfoliate and thereby accelerate damage; (3) it must allow water vapor to migrate freely into and out of the stone so that there is no accumulation of water behind the treated layer, which would accelerate damage to the statue; and (4) it must increase the strength of the treated layer to a considerable degree.

In addition to the selection of suitable chemical consolidants, nondestructive measurements of the depth of weathering and of penetration of the consolidant are critical. This problem has been solved by the development of an electrical resistivity method and the application of a C-1 microdepth measuring instrument.

Principles and Testing Validation

Electrical resistivity of a medium is directly related to its density and other physical properties. After weathering, the resistivity of rock undergoes great changes, and there are marked differences in the resistivity of the same rock type that has undergone both severe and mild weathering. Chemical consolidation also changes the resistivity of the rock. Therefore, measurement of resistivity can provide information on the depth of weathering and penetration of the consolidant. Even the depth of penetration of different components of mixed materials can be determined.

As shown in Figure 1, two electrodes, A and B, are attached to the surface of the rock, and a direct current of intensity I is passed into the rock. Electrodes M and N are attached at two additional points and the

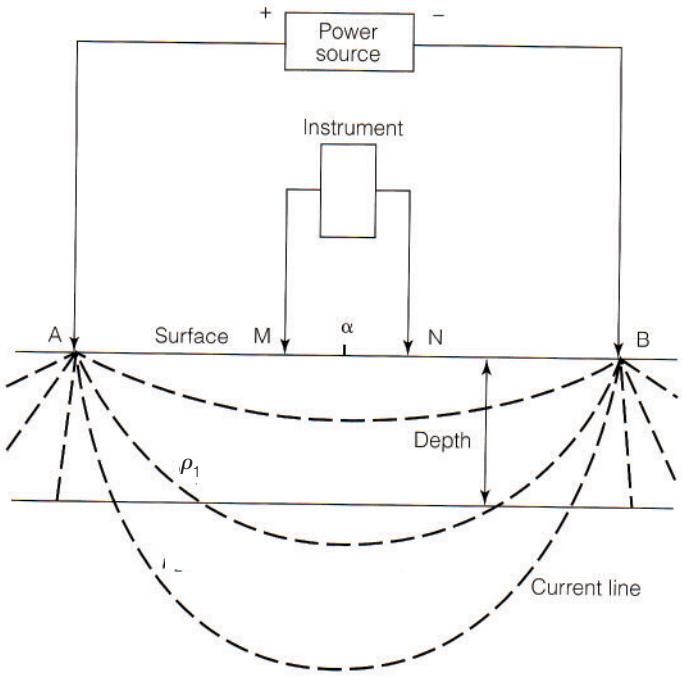

Figure 1
Principle of the resistivity method of weathering depth determination.

potential difference $\triangle V_{MN}$ determined. The resistivity, ρ_S, of the rock can be calculated by the formula

$$\rho_S = K \triangle V / I$$

where K is a constant calculated on the basis of the relative positions of A, B, M, and N, and ρ_S represents the conductivity of the medium at a certain depth. When the current at A and B is increased, the value of ρ_S reflects the increase in depth. The depths of layers of different resistivities can then be determined from a ρ_S–h plot, where h represents depth within the stone.

This method is used to measure depth of weathering of rock and the penetration of the chemical consolidant. It can also be used for nondestructive determination of the thickness of, for example, a concrete layer on the surface of carved rock or the depth of a mud-plaster or lime-mortar layer.

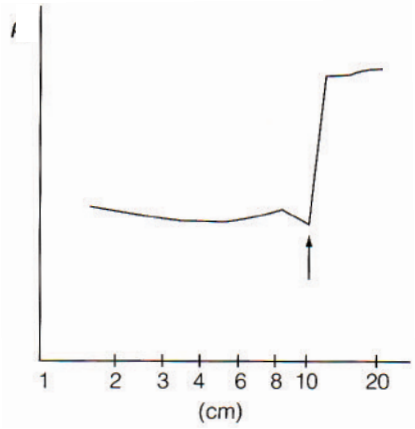

Figure 2
Resistivity curve to determine thickness of an applied layer of concrete on rock.

Figure 2 shows how the depth of a concrete layer over a rock surface may be determined. The curve compares the results of the method with measurements after drilling and corroborates the effectiveness of the method. Furthermore, since the thickness of the concrete layer ranged from 10 to 25 cm, the precision of measurement could be selected in a range of about 1 cm. A probe of measurement precision of 2–3 cm can therefore be used for measuring depths of weathered layers and of chemical penetration only 2–3 mm in thickness.

On-Site Measurements

A configuration of four symmetric electrodes was used for on-site measurements on carved rock surfaces. That is, A, B, M, and N were arranged

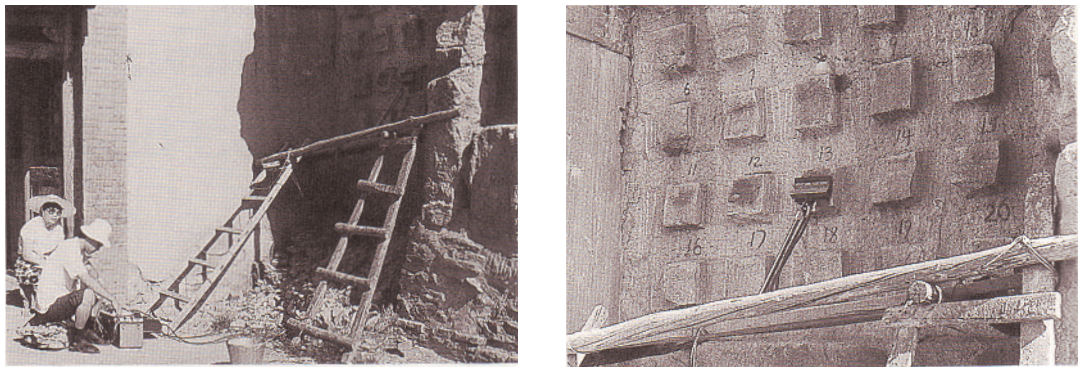

a b

Figure 3a, b
On-site measurement: (a) instrumental setup; and (b) close-up showing attachment of electrodes.

in a straight line, so that A and B were symmetrical to the midpoint, O, between M and N; that is, AO = BO. Then,

$$K = 2\pi AM \cdot AN / MN$$

To facilitate measurement, electrodes were affixed in advance to an insulated frame according to predetermined sizes of AN and MN. To provide an adequate fit on uneven surfaces, each electrode group was spring-loaded for good contact with the surface. An electrode with a diameter of 2–4 mm is used to measure depth of about 10 cm; for measurements in the range of 2–3 cm with a precision of 2–3 mm, an electrode of 0.5–1 mm is used.

Because the contact resistance between the electrodes and the surface of the carved rock was found to be higher than 200 kΩ, ordinary measuring instruments could not be adapted. The C-1 microdepth measuring instrument developed by the authors was designed for a specific purpose, and normal determinations were possible even when electrode ground resistance was as high as 500 kΩ. The instrument is also light and convenient, and it consumes little electricity.

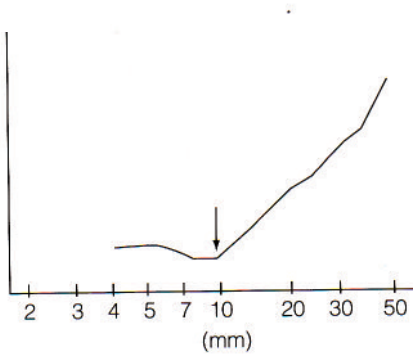

Figure 4
Curve showing 10 mm weathering depth on carved rock, Yungang grottoes.

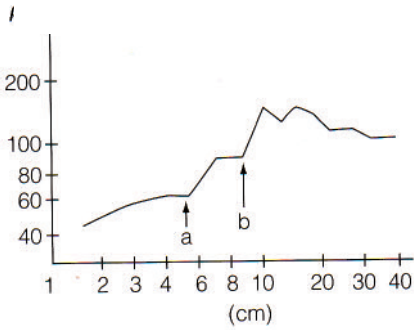

Figure 5
Curve determined on the Great Buddha statue at Leshan: a = depth of severely weathered zone; b = depth of weathered zone.

This nondestructive technique for determining the depth of weathering of rock and the depth of penetration of consolidants has been applied at the Yungang, Longmen, Kizil, and Dazu grottoes, as well as to the Leshan Buddha statue (Fig. 3a, b). Figure 4 is a curve measured at an experimental site at Yungang. The rock is sandstone, the surface of which was severely weathered. From the curve, it can clearly be seen that the weathering depth was 10 mm. This is consistent with the measurement taken from a cross section of this sculpture.

Figure 5 shows data on the depth of weathering of the sandstone measured on the body of the Leshan Buddha. A depth indicative of severe weathering can be clearly seen.

Figure 6 shows results from the surface of the sandstone adjacent to the foot of the Buddha on the northern wall of Cave 16 of the Yungang grottoes. An abundant accumulation of salt near the surface layer of the sandstone has caused severe weathering to a depth of 10 mm. At a depth of 20 mm, a distinct interface is present parallel to the peeling and

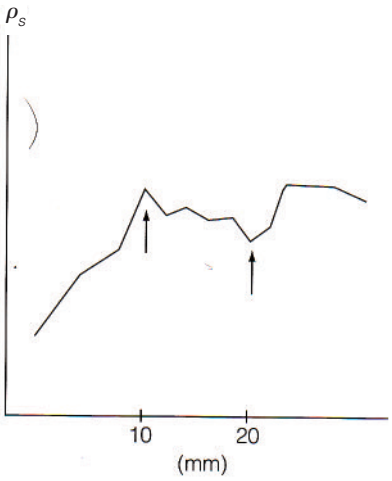

Figure 6
Measured curve at the Yungang grottoes. Severe salt accumulation occurs to a depth of 10 mm; exfoliation occurs at 20 mm.

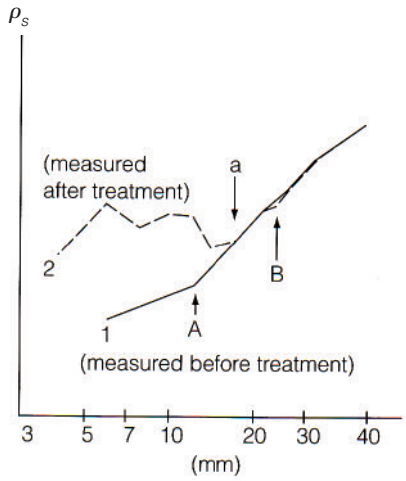

Figure 7
Effects of consolidants on resistivity curves: Curve 1, before consolidation; Curve 2 after consolidation.

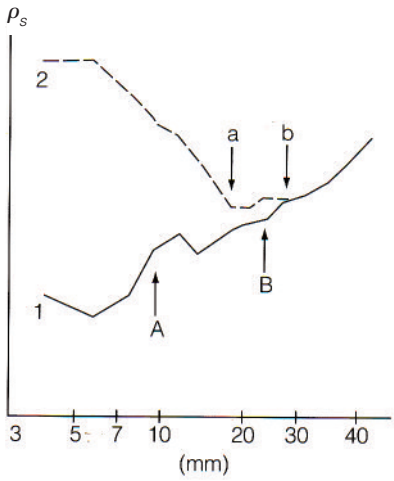

Figure 8
Effects of two different consolidants on resistivity.

cracking on the surface of the wall. These findings are consistent with the results of actual observations.

As stated previously, after consolidant has penetrated the surface of the rock and has solidified in it, resistivity is frequently increased. Organic materials, in particular, cause the resistivity to increase considerably. Therefore, the depth of penetration of the chemical agent can clearly be determined from the initial high resistivity on the measured curve and from a comparison of the same points on the curve before and after applying consolidant. Figures 7 and 8 show curves for the two determinations. Curve 1 in Figure 7 was determined before application of the consolidant, and Curve 2 was determined after its application. Curve 1 in Figure 7 reflects a weathering depth of 12 mm (A) and a less severe weathering depth of 24 mm (B). Curve 2 reflects penetration of the chemical agent (a) to a depth of 17 mm. In Figure 8, Curve 1 reflects a weathering depth of 10 mm (A) and a less severe weathering depth of 24 mm (B). Curve 2 reflects penetration of one chemical consolidant (a) to a depth of 17 mm and penetration of a different consolidant (b) to 28 mm.

Measurements on Test Blocks

Test blocks have relatively small volumes and can easily be moved and immersed in water. For this reason, the two-electrode arrangement method was used (Fig. 9). Three blocks were treated with different consolidants (Table 1). Determinations were made on various planes of the test blocks; specifically, the two electrodes A and M were arranged parallel to the surface, and the electrodes B and N were set at a distance. The test blocks were then submerged in water and the resistivity of the rock was determined at different depths. Because the test blocks were submerged in water, water permeated the weathered layers of the test blocks, lowering resistivity. On this basis, the depth of weathering was determined from the

Table 1 Test results using different consolidants

Consolidant	Thickness (mm) Weathered layers[a]			Penetration depth[b]	
	A layer	B layer	C layer	a layer	b layer
Potassium silicate (PS) No. 1[c]	12	24		17	
PS No. 2	12			6	
PS No. 3	10	28		14	
Methyltrimethoxysilane No. 1[d]	12	20		32	
Methyltrimethoxysilane No. 2	10	17		20	
Methyltrimethoxysilane No. 3	8	17		24	
Methyltrimethoxysilane No. 4	10			32	
Methyltrimethoxysilane No. 5	8	12		24	
PS and methyltrimeth-oxysilane No. 1[e]	10	20	38	20	38
PS and methyltrimeth-oxysilane No. 2	10	24		17	28
PS and methyltrimeth-oxysilane No. 3, test point 6	8	17		8	28
PS and methyltrimeth-oxysilane No. 3, test point 7	8	24		17	28
PS and methyltrimeth-oxysilane No. 4	8	14		20	28
PS and methyltrimeth-oxysilane No. 5	10	20		28	38
Methyltrimethoxysilane No. 1[f]	14	24		14	38
Methyltriethoxysilane	12	24		17	38

Notes

[a] A = severely weathered; B = moderately weathered; C = less weathered.

[b] Penetration depth of consolidants.

[c] Potassium silicate inorganic consolidants of different molar ratio (silica : potassium) and different concentrations in aqueous solution.

[d] Organic consolidants Nos. 1–5 are of different concentrations. [No further information was available from the authors with regard to the composition or method of application. Ed.]

[e] Organic consolidant was applied first, followed by the application of the inorganic consolidant.

[f] Methyltrimethoxysilane was applied first, followed by the application of the methyltriethyloxysilane.

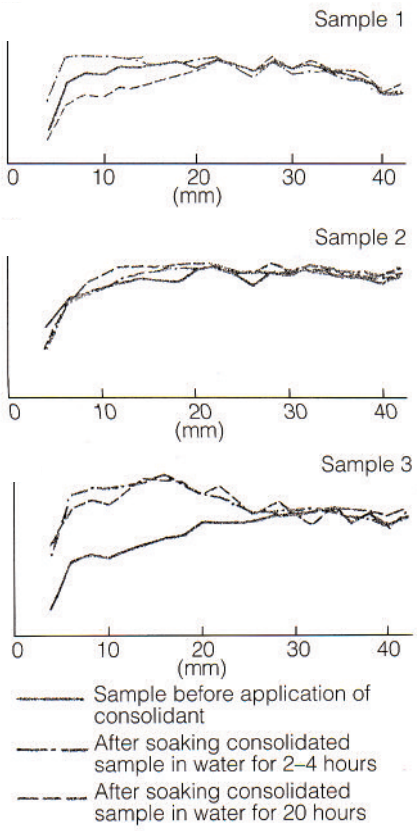

Figure 9
Resistivity curves for laboratory samples, showing consolidant penetration depth in millimeters.

measurement curve. For example, as shown in Figure 9, the depths of severe weathering of samples 1, 2, and 3 were 10 mm, 12–14 mm, and 10 mm, respectively, and the depths of moderate weathering were 12 mm, 20 mm, and 20 mm, respectively (Table 2). By comparing the differences in resistivity before and after the spraying with consolidation, the depth of penetration was determined.

Comparison of the differences in resistivity before and after application of a consolidation in the same test block, and after two hours and twenty hours of soaking, allows differentiation of the water-absorption capacity when different consolidants are being tested. Large quantities of

Table 2
Summary of data shown in Figure 9.

Sample	Resistivity method (mm)			Visual examination (mm)			Consolidant	Penetration
	A	B	C	A	B	C		
1	10–12		22	12		20–22	PS	good
2	12–14	20	28	14	22	24–26	PS and methyl-trimethoxysilane No. 3	poor
3	10	20	26	12	22	26	PS and methyl-trimethoxysilane No. 1	medium

A = depth of severe weathering.
B = depth of intermediate weathering.
C = penetration depth of consolidants.

water penetrate samples of high water permeability when they are soaked for long periods, causing resistivity to be lower than that of similar samples that absorb relatively little water when soaked for a short time.

However, the length of soaking does not have much effect on the resistivity of samples with poor permeability to water. For example, the resistivity shown in the first segment of the curve for sample 1 was greatly decreased after twenty hours of soaking, indicating that the sample was of good permeability. For sample 2, there was basically no change in resistivity as shown in the first segment of the curve after twenty hours of soaking, suggesting poor permeability. The permeability of sample 3 fell between that of the two other samples.

Conclusion

The resistivity method can be used to measure resistivity of rock surfaces at different depths of carved rock on tangent planes. For this reason, its use in determining the depths of weathering of rock sculpture and the depth of penetration of chemical consolidants applied to rock is feasible. Much of the data presented in this paper was compared with visual determinations and with measurements of drilling, and results confirmed that the method can satisfy the requirements of actual fieldwork. The equipment and measuring instruments developed were tested and used extensively in work on grottoes and carved rock. The resistivity method and the C-1 microdepth measuring instrument are also suitable for nondestructive measurements of the thicknesses of covering layers of concrete, lime, and argillaceous matter on rock and carved rock.

Investigations of the Deterioration and Conservation of the Dafosi Grotto

He Ling, Ma Tao, Rolf Snethlage, and Eberhard Wendler

This article describes part of an interdisciplinary, joint Chinese–German project on the preservation of the Dafosi grotto. It focuses on the properties of the sandstone, the influences of moisture and salts on the deterioration of the walls, and preliminary results on the conservation of the stone site. Aspects of Dafosi's art history, polychromy, stability, and rock mechanics are discussed elsewhere in this volume.

The following general description of the topography and geology of the area is based on the *80,000 Signs Report: The Study and Survey of the Environmental and Geological Situation and Deterioration of Dafosi Cave in Bin Xian* (1991). Dafosi is situated in the loess plain in the northern part of Shaanxi Province, near the city of Binxian. The landscape is characterized by the broad valley of the Jing River, which cuts into the yellow earth and the underlying red Cretaceous sandstones. The grotto itself is excavated into the red sandstone of the valley flanks (Fig. 1). The stone floor of the grotto is covered by flood sediments of approximately 2 m thickness, which have been produced by periodic flooding of the Jing River throughout its history.

The sandstone is overlaid by loess layers of the Quaternary period (early, middle, and late Q3). The geological profile shows a horizontal layering of the strata with 180 m vertical distance between the base of the valley and the top of the hill. The height of the sandstone rock is 55 m. Typical for sandstone in general, clay-stone layers of various thicknesses are interspersed between the sandstone rock series. These layers form impermeable barriers against the water that flows from the top of the hill along the fissures as well as through the rock itself.

One of these clay-stone layers intersects the Dafosi grotto about 2 m above the present ground level, with an intersection length of 65 m. The water that seeps out of this horizon layer trickles into the sediment layers covering the floor. This seepage water is the main source of deterioration of the statues and the walls inside the grotto. The sandstone is particularly damaged along the clay-stone horizon. Behind the Great Buddha in the grotto, the sandstone is eroded back to 2.5 m from its original surface.

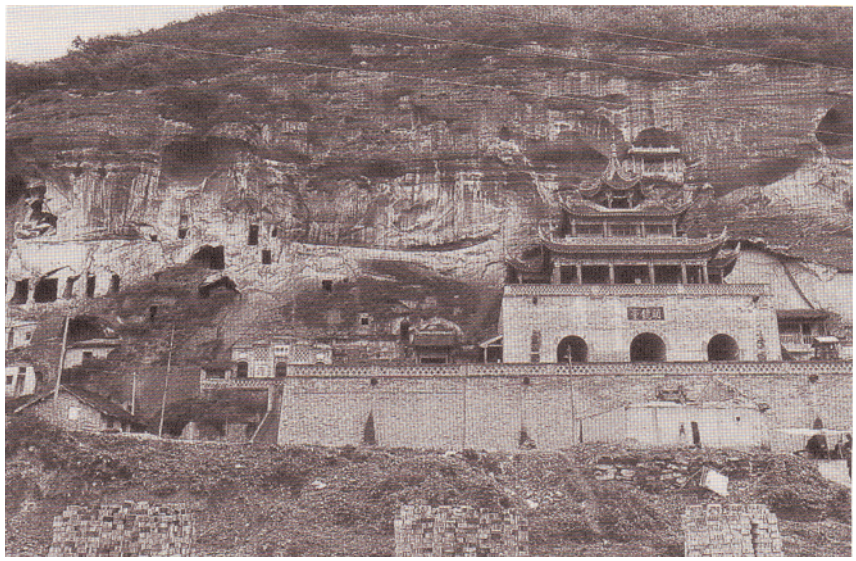

Figure 1
View of the Dafosi grotto.

Weathering of the sandstone walls

The weathering of the sandstone walls inside the grotto can be divided into four vertical zones (Fig. 2), described as follows from bottom to top:

Zone A (0–2 m): Thin sandstone layers separated by thin clay-stone layers. The sandstone is cracked into small blocks. The moisture content is high; there is little or no salt efflorescence. The top of Zone A is formed by a thick clay-stone layer. Nos. 1–3 drill-core and scraping samples are from this layer.

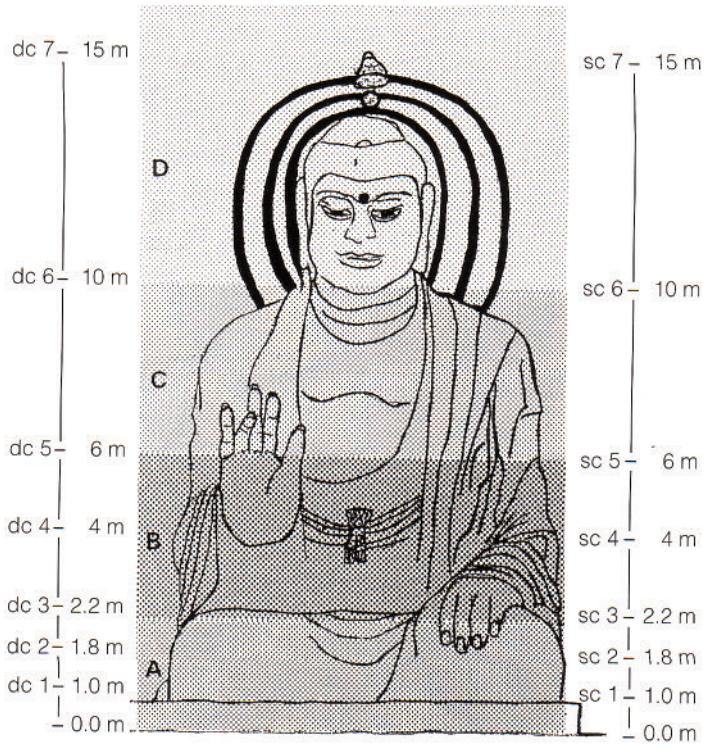

Figure 2
Schematic drawing of the Great Buddha and the locations of sampling: dc = drill core; sc = scraping sample from the surface. Shaded areas A–D show the level of deterioration, which is highest in Zone B, lowest in Zone D.

Zone B (2–6 m): Thick sandstone layers separated into large blocks. This zone is situated in the dynamic area of water migration and evaporation. Heavy erosion is evident at the clay-stone layer. Thick salt crusts and efflorescence can be found. Nos. 4 and 5 drill-core and scraping samples are from this layer.

Zone C (6–10 m): Thick sandstone layers separated by fissures. This zone is situated in the migration area of the most soluble salts and determines the upper limit of salt and moisture action. The moisture content is low, displaying little salt crusting or efflorescence. No. 6 drill-core and scraping samples are from this layer.

Zone D (10–23 m): Thick sandstone layers are separated by fissures. There is good ventilation. No salt crystallization is found. Remains of former wall paintings have been found in this area. No. 7 drill-core and scraping samples are from this layer.

The degree of deterioration is greatest in Zone B. To investigate the properties of the sandstone, samples were taken according to the stone varieties and the deterioration sequence at heights of 1, 2, 4, 6, 10, and 15 m. Two types of samples were taken: drill-core samples 2 cm in diameter and 30 cm in length taken from the wall at the left side of the Buddha, and scraping samples from the wall on the statue's right side. Eight soil samples were also taken to determine the salt content of the ground. Figure 2 shows the location of the drill-core and scraping samples.

Sandstone Types and Their Hydrological Properties

The following investigations were carried out to determine the physical and chemical properties of the stone types: microscopic thin-section analysis; measurement of density and of transport parameters of liquid water, water vapor, and moisture dilatation; and measurement of water-vapor absorption (sorption isotherm). The results are compiled in Table 1. Table 2 contains a comparison of selected properties before and after treatment with stone strengthener.

Table 1 Hygric properties of sandstones in Dafosi

No.	Height (m)	Rough density (g cm^{-3})	Porosity (vol. %)	H_2O (npr) (vol. %)	H_2O (vac) (vol. %)	W (kg m^{-2} $h^{-1/2}$)	B (cm $h^{-1/2}$)	W/B (kg m^{-3})	Vapor diffusion [μ (–)]	Hygric dilatation (μm m^{-1})
1	1	2.29	15.0	8.9	15.0	1.0	n.d.	n.d.	32	240
2	1.8	2.30	15.3	9.2	15.3	1.3	1.8	75	20	330
4	4	2.02	24.0	15.2	24.0	37	26	142	17	720
5	6	2.06	22.7	13.1	22.7	11	10	117	n.d.	400
6	10	1.91	28.5	18.0	28.5	36	24	158	13	520
7	15	1.96	26.7	17.1	26.7	20	14	142	14	370

Table 2 Properties of consolidated sandstones in Dafosi

No.	Height (m)	H_2O (npr) (vol. %)	W (kg m^{-2} $h^{-1/2}$)	Vapor diffusion [μ (−)]	Hygric dilatation (μm m^{-1})	Pull-off strength (N mm^{-2})
2	2	4.0 (9.1)	0.4 (1.3)	60 (20)	250 (320)	2.2 (1.9)
4	4	5.9 (15.2)	1.0 (37)	21 (17)	890 (720)	0.7 (0.5)
6	10	6.2 (13.1)	0.8 (11)	30 (19)	1000 (400)	0.9 (0.8)
7	15	5.5 (17.1)	0.7 (20)	33 (14)	320 (370)	0.8 (0.4)

Generally, the binding material of all the sandstone varieties studied is rich in clay and ferrous compounds, but the sandstones differ significantly below and above the clay-stone layer. Below the clay-stone horizon, the sandstones are matrix-rich, partly carbonate, and partly clay-rich; the grain size in this area is much smaller than in the upper zones. The sandstones above the clay-stone layer are grain-supported with a much greater visible porosity. The red color in this region is caused by ferric oxide clay layers coating the sand grains. Chlorite is the main clay mineral of the sandstones above the clay-stone layer, whereas illite and kaolinite prevail below it.

The moisture-transport properties of the sandstone indicates that the porosity of the sandstone increases with height, as shown in Table 1. The varieties below and above the clay-stone layer (at the top of Zone A) are very different in this respect. This behavior is expressed by the water-uptake coefficient W (kg m^{-2} $h^{-1/2}$) and the water-penetration coefficient B (cm $h^{-1/2}$). Both values were measured according to DIN 52617. The sandstone varieties in the upper part of the grotto show extremely high values of W and B. This explains the wide distribution of moisture and salts over the walls of the grotto. The dilatation (expansion of the stone when immersed in water, DIN 52450) was particularly enhanced in sample 4, located at a height of 4 m directly above the clay-stone layer. This maximum corresponds with the maximum salt content. It is known from many experiments that gypsum content significantly increases the dilatation of sandstone (Möller, Wendler, and Schuh 1992).

Water-vapor sorption isotherms (DIN 50008) at 20 °C were determined for six sandstone varieties. The isotherms shown in Figure 3 are of the same type and plot very close together. The absorbed water content increases continuously with increasing relative humidity. The sorption isotherms do not seem to be influenced by the salt content of the stone, however. This confirms the result that—besides gypsum and calcite, which are not hygroscopic—no other salts in major concentrations occur in the sandstone (Fig. 4).

The Distribution of Soluble Salts

Soil samples, drill cores, and surface-scraping samples were taken to identify the salts and their distribution in the grotto. Drill cores were sliced into sections to determine the depth distribution of the salts.

Figure 3
Water-vapor sorption isotherms (20 °C) of the sandstone types. LiCl = 12% RH; $MgCl_2$ = 35% RH; $NaNO_3$ = 65% RH; NaCl = 76% RH; KNO_3 = 93% RH.

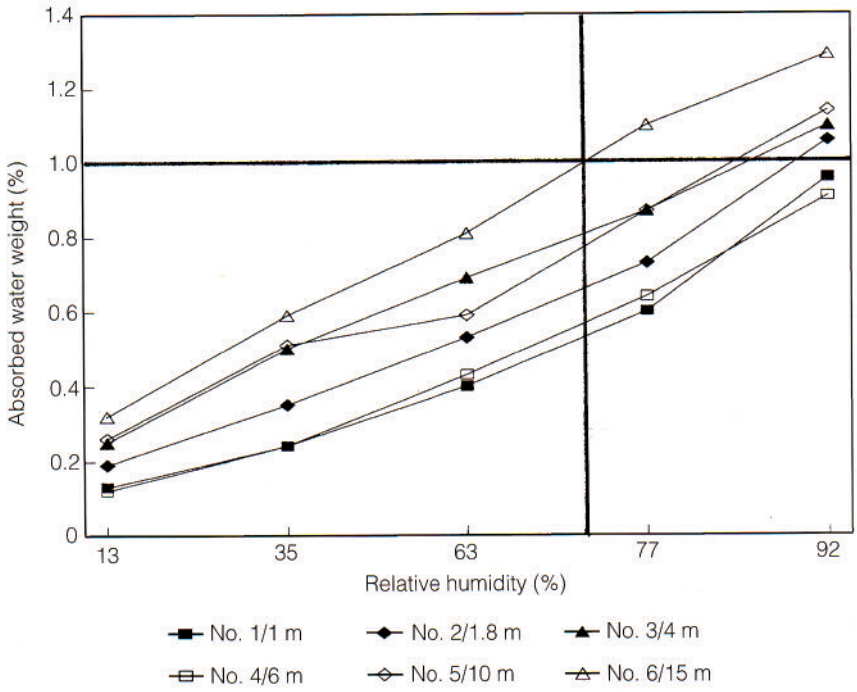

Figure 4
Vertical height profile of water soluble ionic species in the surface of the sandstone walls. Note the logarithmic scale in the anion's diagram.

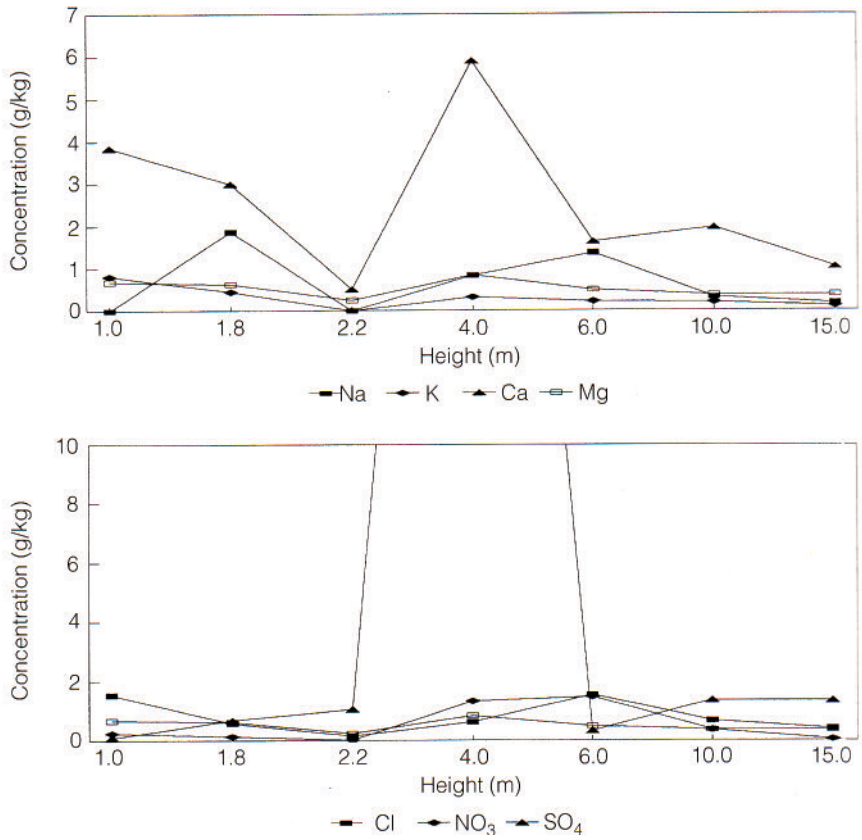

In addition to river sediments, the floor of the grotto contains debris from the deterioration of the sandstone walls. The moisture content and salt content of the soil are quite high; the moisture content is 3–16 weight % with a mean of approximately 7–8 weight %. The principal

ions found are calcium and sulfate in a concentration of 5–10 g/kg. Nitrate and chloride are also present.

The vertical salt profile shows a characteristic zoning (Fig. 4). Salts are enriched in the zone between 2 and 6 m, which corresponds to the capillary rise of moisture above the clay-stone layer. The increase in calcium below that layer can be explained by the influence of water seepage from that region. From 6 to 15 m below that layer, the content of soluble salts is almost constant. The distribution of salts coincides with the extent of damage to the sandstone walls, as illustrated in Figure 2.

The total ionic content found in the sandstone is not very different from that of the soil samples. Calcium and sulfate (gypsum) are the main ions. Nitrate is slightly more enriched in the soil samples than in the drill-core samples. The balance of the total ionic species soluble in water further indicates the presence of sodium and magnesium salts.

Salt efflorescence collected in the grotto was analyzed by X-ray diffraction and found to consist of gypsum and calcite. The same salts also crystallized from the eluates used to determine the anion and cation profiles. The presence of gypsum can be explained by the reaction of dissolved calcium hydrogen carbonate with sulfate-containing rainwater and groundwater. Because the loess contains large amounts of calcite, which is dissolved by rainwater, this result clearly demonstrates that both of these salts are transported by the water seeping from the top of the hill through the sandstone rock.

Depth profiles of water-soluble ionic species were analyzed to determine the distribution of salts in the interior of the sandstone. The profiles are typical for the prevailing climatic conditions. Near the ground, where there is little evaporation, a homogeneous depth distribution is found. At a height of 4 m, in the dynamic zone of wetting-drying cycles, the salts are enriched on the surface of the sandstone. The salt content decreases significantly with increasing height.

The salt content in the rock is low to medium compared to the total porosity of the sandstone, which is in the order of 25 volume %. The main salts found, gypsum and calcite, are not hygroscopic. Therefore, the moisture content in the stone is caused by seeping rainwater and moisture condensation due to the climatic conditions.

Climatic Measurements

Measurements carried out since 1992 show that the daily variations of temperature and relative humidity directly outside the grotto are buffered inside. Near the ground, the temperature is always very close to that of the dew point, so condensation conditions prevail. With increasing height, ventilation and drying conditions improve; consequently, inside and outside temperatures and relative humidity levels are similar. On the basis of mean monthly data, the dew-point interval (the difference between air temperature and dew-point temperature) was calculated inside the grotto (Fig. 5). Results show that the interval between the inside temperature and the dew point is less in the spring and summer and more during the autumn and winter months. The latter period can, therefore, provide good drying conditions with better possibilities for conservation measures.

Stone Consolidation

Until now, only a few experiments have been carried out with original Dafosi material (Table 2). The treatment with Stone Strengthener Wacker OH (tetraethoxysilane) causes some evident changes of stone properties: the water uptake coefficient is lowered, as is the water uptake under normal pressure. This result can be explained by the deposition of SiO_2 gel in the pore space, which remains hydrophobic for some weeks after the treatment. Corresponding to that result, the water-vapor-diffusion resistance number is increased. Dilatation is also increased, though only slightly. Because of the size of the samples available, only the pull-off strength according to DIN 18555, part 6 could be measured; the results showed a clear increase. Future experiments will be undertaken to develop an adapted stone-consolidation program using Wacker OH and formulations containing diethoxy-dimethylsilane (DEX-DMS) as a plasticizer for the SiO_4 tetrahedral network.

Suggestions for Further Research and Intervention

Origin of the seepage water

Using the porosity and capillarity data measured, the transport paths of the seepage water can be approximated. Microscopic thin-section analysis shows the size of the macropores of the sandstone above the clay-stone layer to be ±0.1 mm. Using this figure, the height of capillary rise of water in these pores can be calculated as approximately 0.2 m. When the water column in the stone is longer than approximately 0.2 m, however, the pore water migrates downward and trickles out of the pore system. The rocks of the upper series in the Dafosi grotto can, therefore, be classified as good moisture conductors (*80,000 Signs Report* 1991). Rainwater is quickly conducted downward through the massive rock sequences. Then the water seeps out along fissures, and most of it is transported along these paths. Finally, all migrating water collects at the clay-stone layer. These different transport paths probably cause the water to originate from an extensive area on top of the hill. Therefore, the installation of a geotextile (water-impermeable membrane) to control the seepage does not appear to be practical.

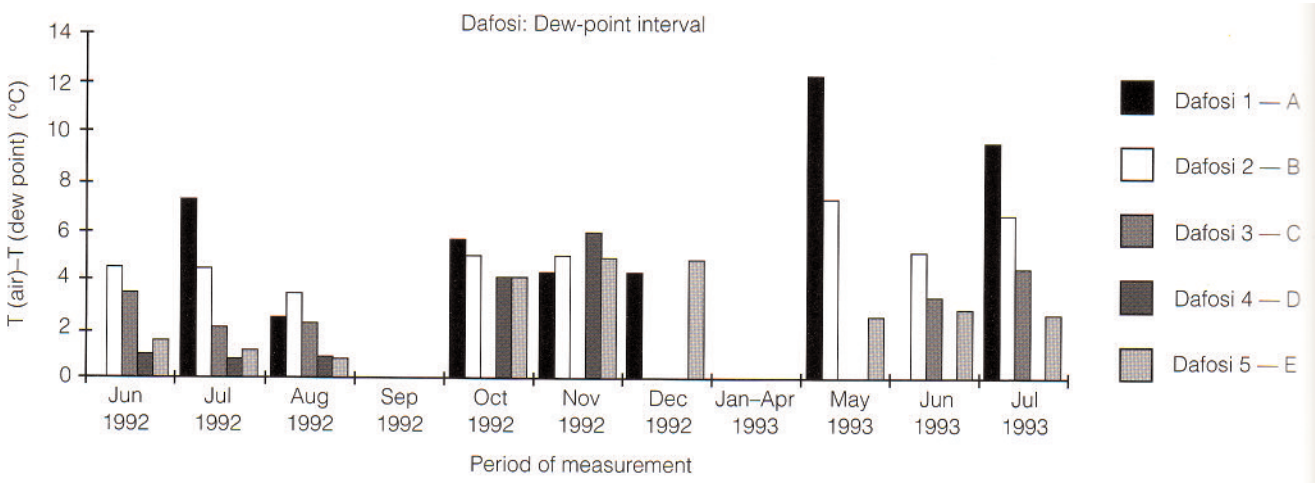

Figure 5
Air temperature–dew-point temperature interval at different levels in the grotto. Location of the records: Dafosi 1 = outside air in front of the grotto; Dafosi 2 = 10 m; Dafosi 3 = 8 m; Dafosi 4 = 2 m behind the Buddha; Dafosi 5 = 0 m, on the floor.

Reducing moisture in the grotto

The primary challenge to preventing further deterioration of the site will be to lower the humidity inside the grotto by diverting water seepage. For this purpose, the eroded space along the clay-stone layer will be closed by a wall, and the water that collects behind the wall can then be drained by tubes. As an additional measure, sediments covering the grotto floor will be removed as a means of increasing the evaporation area and lowering the salt contamination of the grotto as a whole.

Stone conservation in the grotto

Although the damage observed is extensive, the following factors may facilitate the conservation of the sandstone: The main salts present are gypsum and calcite; since these salts are not hygroscopic, they do not contribute to an increase in the moisture content of the stone. The salt content is moderate to medium compared to the total porosity of the stone, and the salts are concentrated in the outer 5–10 mm. Sacrificial mortar layers are able to displace the evaporation zone, simultaneously displacing the accumulation of salts from the stone surface into the rendering. With time, some extraction of the present salts can be expected, although gypsum and calcite are quite insoluble.

Because neither gypsum nor calcite are hygroscopic, the moisture of the stone is determined primarily by the amount of seeping water and condensation from the air. Sorption isotherms, therefore, give an indication of the appropriate conditions for conservation. Figure 3 shows that when the relative humidity is below 75%, the amount of absorbed water is less than 1 weight %, which is low enough to obtain a sufficient penetration depth of stone consolidants. For this reason, it is absolutely necessary to monitor the climate in the grotto and wait for these appropriate conditions. Yet treatments can be carried out only after a long dry period. Karsten pipe measurements can help determine whether uptake-and-penetration depth of a stone consolidant is sufficient (Wendler and Snethlage 1989).

In the near future, conditions appropriate for the application of a stone consolidant can be expected for only the upper parts of the grotto. The treatment, therefore, will be carried out in two or three steps. The upper areas, which are already sufficiently dry, will be treated first. Then, after the removal of the floor sediments and the control of the seeping water with drainage tubes, the lower walls will be allowed to dry out for several years. When dry, the remaining areas of the grotto can also be treated.

Acknowledgments

The investigations reported in this chapter were financially supported by the Federal Ministry of Research and Technology, Germany; and the Ministry for the Preservation of Cultural Property of Shaanxi Province, People's Republic of China.

References

DIN 18555, part 6, 11.87: Prüfung von Mörteln mit mineralischem Bindemittel. Festmörtel. Bestimmung der Haftzugfestigkeit.

DIN 50008, 07.81: Konstantklimate über wäßrigen Lösungen. Teil 1: Gesättigte Salzlösungen.

DIN 52450, 08.85: Prüfung anorganischer nichtmetallischer Baustoffe. Bestimmung des Schwindens und Quellens an kleinen Prüfkörpern.

DIN 52617, 05.87: Bestimmung des Wasseraufnahmekoeffizienten von Baustoffen.

Institute of Survey of the Technical and Electrical Ministry and the Shaanxi Provincial Center for the Preservation of Cultural Property

1991 *80,000 Signs Report: The Study and Survey of the Environmental and Geological Situation and Deterioration of Dafosi Cave in Bin Xian* (October). Xian: Institute of Survey of the Technical and Electrical Ministry and the Shaanxi Provincial Center for the Preservation of Cultural Property.

Möller, U., E. Wendler, and H. Schuh

1992 Längenänderungsverhalten hydrophobierter Sandsteine. *Bautenschutz und Bausanierung* 15(4):45–49.

Wendler, E., and R. Snethlage

1989 Der Wassereindringprüfer nach Karsten: Anwendung und Interpretation der Meßwerte. *Bautenschutz und Bausanierung* 12(6):110–15.

Color Change of Pigments in the Mogao Grottoes of Dunhuang

Nobuaki Kuchitsu, Duan Xiuye, Chie Sano, Guo Hong, and Li Jun

As is typical of old mural paintings, the art in the Mogao grottoes of Dunhuang has undergone discoloration or color change. A dark brown material has been observed in many paintings, particularly in portrayals of human skin. In some cases, the skin looks black. These dark colors are thought not to be the original colors applied to the wall. Art historians note that, as the Mogao grottoes are located in northwest China, the skin was likely to have been originally painted in yellow. Color change is therefore suspected. It is well known that local people lived in some of the cave temples, as evidenced by soot deposits on the wall paintings, but this is different from the darkening of specific parts of paintings. Accordingly, it is important to analyze the mineral pigments believed to have undergone color change to determine the original colors and to prevent further alteration in the future.

Previous Work

The color change of pigments in the Mogao grottoes has been studied by Duan and coworkers (e.g., Duan 1987; Duan et al. 1987) and Li (1992). They noted that minium (Pb_3O_4) sometimes changes into plattnerite (PbO_2) (i.e., orange changes into black) on some mural paintings. Substantial microscopic observation of a dark brown sample from the painting of human skin in Cave 205 (Tang dynasty) revealed that it is divided into two layers: a thin surface black layer and the dominant inner orange layer. The black layer corresponds to plattnerite, and the orange layer corresponds to minium. The original depiction of human skin had surely been painted a cream color, where orange was added to an initial white coat, but oxidation of minium into plattnerite changed the color to dark brown. This transformation is important not only to art historians but also to conservators of wall paintings. Because oxidation is not the only threat to pigments, it is necessary to analyze and describe the many cases of color change of pigments.

Samples

Cave 194 was surveyed for color change. This cave temple was excavated in the Tang dynasty and partially repainted in the Xixia dynasty. At least five

colors present in the wall paintings are recognizable and have not suffered significant color change: red, green, yellow, black, and blue. Dark brown parts distinguishable from soot are also present. Though the paintings have been severely damaged by salt crystallization, the pigments themselves appear hardly changed, except for the dark brown areas. Sampling of the pigments in this grotto was conducted at two points on the south wall of the main chamber. The dark brown and green pigments are the focus of the following observations.

Methods

After samples were embedded in resin, a cross section was observed under a high-powered microscope. Chemical analyses were conducted using a JEOL JSM-840A with JEOL JXA-840A electron probe microanalyzer (EPMA). Measuring conditions were 15 kV and 1×10^{-8} mA. Mineralogical analyses were also undertaken through examination by X-ray diffraction (XRD) using a JEOL-3500-DX-MAP2 instrument. The measuring conditions were 30 kV and 400 mA, and the diameter of the microbeam was 100 μm. Both copper and chromium were used as the radiation sources.

Results

Dark brown sample

EPMA data are shown in Figure 1a–c. Microscopic observation of the cross section of the dark brown sample revealed that it is composed of two parts: the main part, which is red; and a very thin surface layer, which is black (Fig. 1a). The distribution of iron concurs with the pigment layer (Fig. 1b). The distribution of sulfur concurs with the outer margin of the pigment layer, which corresponds to the black surface layer (Fig. 1c). XRD data are shown in Figure 2. Pyrite (FeS_2) and hematite (Fe_2O_3) have also been identified as components of the sample, a result that is consistent with the EPMA data.

Green sample

Examination of the cross section shows that the green pigments have been partially dissolved into the embedding resin, leaving them bluish and rather ambiguous. The pigment layer, however, is still recognizable. EPMA data for the green sample are shown in Figure 3. The distribution of chlorine agrees with that of copper, which corresponds to the pigment layer. Moreover, the distribution of sulfur also agrees with that of copper. XRD analyses show that the green sample is composed mainly of atacamite, $Cu_2Cl(OH)_3$, with minor amounts of antlerite, $Cu_3SO_4(OH)_4$, consistent with the EPMA data.

Discussion

Although hematite is common as a red pigment, pyrite is not. Therefore, it is thought that the dark brown sample was originally red and composed of hematite. The subsequent formation of the black surface layer, composed of pyrite, caused the color to change to dark brown. If this is indeed the

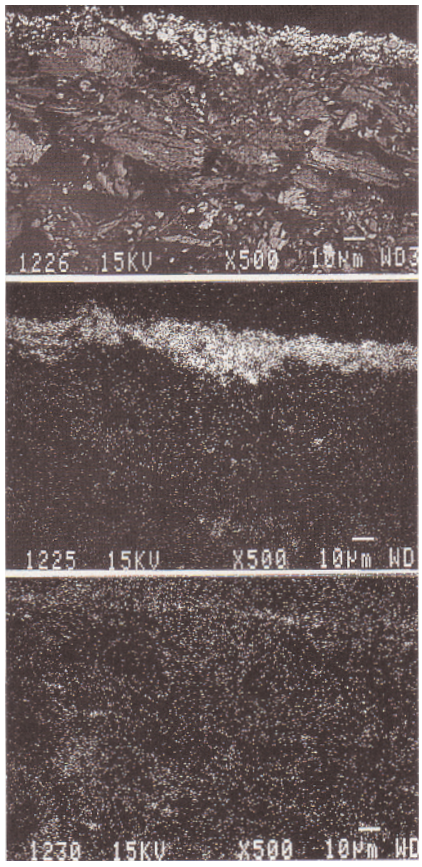

Figure 1a–c
Elemental distribution map of the cross section of dark brown pigment in Cave 194 by EPMA, in which (a) the bright part corresponds to heavy elements, the dark part corresponds to light elements, and the bright band is presumed to be the pigment layer. The other images show (b) distribution of iron, agreeing with the presumed pigment layer, which is seen as the bright band; and (c) distribution of sulfur, agreeing with the outer margin of the pigment layer.

case, then the cause of this color change can be attributed to the transformation of hematite into pyrite through its interaction with a sulfur-containing compound. It is notable that hematite, which is generally regarded as much more stable than minium, is also subject to change.

Generally, the green pigments in the mural paintings of the Mogao grottoes are regarded as stable because little color change is detectable with the naked eye. However, the green samples of Cave 194 show that there has been some dissolution of the green pigment into resin. This suggests the occurrence of a mineralogical change. Although atacamite is a mineral commonly present in green pigment, antlerite—which is barely distinguishable from atacamite with the naked eye and may be an alteration product of atacamite—may be present. Antlerite is soluble in water. Thus, the green pigments of Cave 194 require consideration of their preservation needs. Consequently, color change is not the only threat to the conservation of mural paintings; mineralogical alteration should

Figure 2
X-ray diffraction data of the dark brown pigment in Cave 194. The radiation source is chromium. Peaks labeled A show the existence of hematite (Fe_2O_3); B peaks show the existence of calcite ($CaCO_3$); C peaks show the existence of pyrite (FeS_2); D peaks show the existence of quartz (SiO_2). Calcite and quartz are commonly observed in the ground layer of mural paintings. Hematite and pyrite are identified as the main components of the pigment layer.

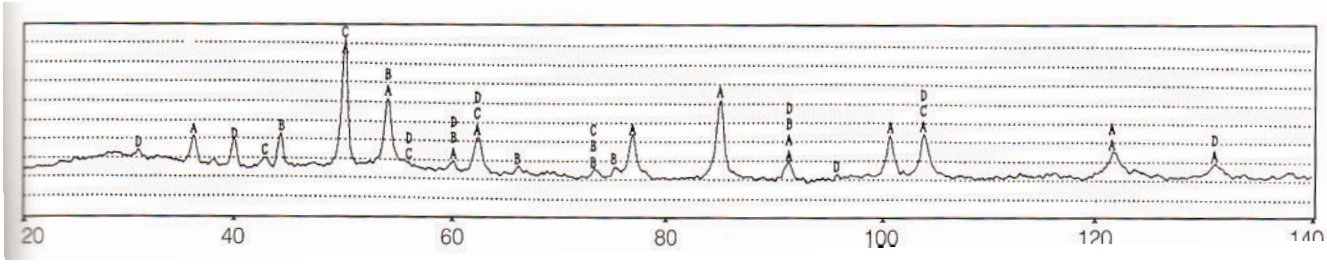

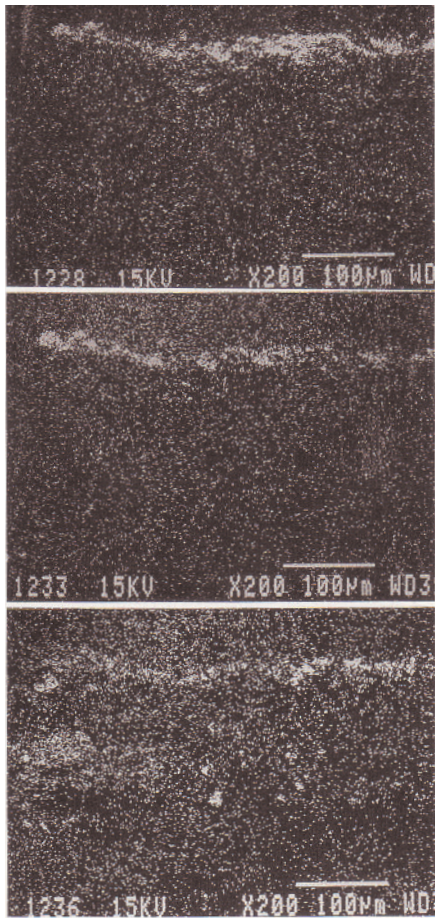

Figure 3a–c
Elemental distribution map of the cross section of green pigment in Cave 194, in which (a) the distribution of copper corresponds to the pigment layer; (b) the distribution of chlorine is consistent with the distribution of copper; and (c) the distribution of sulfur also agrees with the distribution of copper.

also be considered, and it is necessary to understand the precise condition of the pigments when considering the preservation of mural paintings.

In both cases, sulfur plays an important role in the deterioration of pigments. The origin of the sulfur has not yet been ascertained. Its distribution in the cross section suggests that it did not come from the geological strata into which the grottoes are excavated. Because sulfur is found only on the outer part of the pigment layer, it is believed that this element is present in the atmosphere of the cave. It is therefore necessary to determine the atmospheric environment of the Mogao grottoes. While this study has not yet detected significant air pollution in Cave 194, continuous observation is needed.

Conclusion

In Cave 194, the alteration of hematite into pyrite was observed as the cause of a color change from red to dark brown. Although green pigments such as atacamite are regarded as stable, they, too, are subject to alteration. This process does not necessarily cause color change as with the conversion of atacamite into antlerite; nevertheless, the alteration could possibly pose a threat to the conservation of mural paintings. Because sulfur plays an important role in the deterioration of pigments, it is necessary to study how it enters the grotto in order to prevent its contact with the mural paintings.

Acknowledgments

The authors would like to express their sincere gratitude to all the people who assisted in this collaboration between China and Japan.

References

Duan Xiuye
1987 The pigments used in the Mogao grottoes, Dunhuang. *Butsugei* 175:90–100.

Duan Xiuye, Jun-ichi Miyata, Noriko Kumagai, and Ryuitiro Sugisita
1987 Analysis of pigments and plasters from the wall paintings of Buddhist temples in northwestern China. *Scientific Papers on Japanese Antiques and Art Crafts* 32:13–20.

Li Zuixiong
1992 A study of the red pigments used in the Mogao frescoes and the mechanism of their discoloration. *Dunhuang Yanjiu* 32:41–54.

Analysis of Wall Painting Fragments from the Mogao and the Bingling Temple Grottoes

Ian N. M. Wainwright, Elizabeth A. Moffatt, P. Jane Sirois, and Gregory S. Young

In 1988, the Analytical Research Laboratory of the Canadian Conservation Institute, in collaboration with Li Zuixiong of the Dunhuang Academy, undertook the analysis of wall painting fragments from the Mogao grottoes at Dunhuang and the Bingling Temple grottoes near Lanzhou, Gansu Province. A total of thirteen fragments—ten from the Mogao grottoes and three from the Bingling Temple grottoes—were studied. Their precise locations within the caves are not reported here; the fragments were chosen to be representative of the range of colors observed, including white, black, red, blue, beige, green, and purple. The investigation had several objectives, including an examination of the clay and paper supports, characterization of the binding medium of the paint and its deterioration, and analysis of pigments and other inorganic materials. In addition to the thirteen fragments examined, a comparative analysis was undertaken of several raw materials of both plant and animal origin—including fish, bone, and skin glues, and peach pitch. The authors further undertook a review of literature pertaining to the materials of Chinese wall paintings to evaluate processes of site deterioration. The aim was also to share the analytical methods with the Dunhuang Academy for the development of its conservation science program.

A number of studies of pigments and other materials relevant to these analyses have been reported, notably work by Gettens (1938a, 1938b) on Chinese wall paintings including those of Dunhuang (see also Warner 1938), by Delbourgo (1980) on a ninth-century silk painting from Dunhuang, and by Warner at the British Museum, whose results are described in *Buddhist Cave Paintings at Tun-Huang* (Grey 1959). Two unpublished reports by Gettens (1935, 1936), which include experiments on the alteration and discoloration of red lead, are on file at the Fogg Museum of Art in Cambridge, Massachusetts. The authors' laboratory has published results on three wall paintings from the Royal Ontario Museum in Toronto (Moffatt, Adair, and Young 1985), in which calcium oxalates were found. Winter (1984) provides a bibliography on pigments in China, which was invaluable to our research. A review of the causes of deterioration of the Mogao grotto paintings is given by Qi Yingtao (1984).

A parallel project was undertaken at the Dunhuang Cultural Relic Research Institution and published by Hsu Wei-yeh, Chou Kuo-hsia, and Li Yun-ho in *Dunhuang Yanjiu* (1983). Their study was based on the analysis of 293 samples from the Mogao grottoes and showed that the following pigments were used: kaolin, calcium carbonate, lead chloride, lead sulfate, lead chloride carbonate, lead carbonate, quartz, red ocher, hematite, cinnabar, red lead, realgar, azurite, lapis lazuli (including synthetic ultramarine), malachite and copper chloride, graphite, ferric sulfate, gold powder or gold leaf, and mica. The discoloration of red lead and the nature and genesis of copper chlorides in the greens are also discussed.

Methods of Analysis

Cross sections were prepared by embedding fragments in a polyester casting resin and grinding one transverse face, using silicon carbide papers, followed by polishing with alumina on a synthetic velvet lap. Because of the friable and porous nature of the fragments, the embedding plastic was introduced with vacuum impregnation. Sections were examined by polarized light, incident light, and fluorescence microscopy,[1] and by X-ray microanalysis using a scanning electron microscope equipped with secondary and backscattered electron detectors and an X-ray spectrometer.[2]

Debye-Scherrer X-ray diffraction and diffractometry were used to identify the inorganic pigments used. Samples of pigment were mounted on glass fibers using silicone grease and then mounted in Gandolfi cameras. Clay used for preparing the sandstone walls for painting was studied by X-ray diffractometry to determine the major clay mineral constituents present.[3]

The organic component of the paints (i.e., the vehicle or binding medium) was studied by Fourier transform infrared spectroscopy with samples mounted in a high-pressure diamond anvil microsample cell.[4] Difficulties often encountered with this kind of analysis include very low concentrations of organic materials (e.g., less than 3–5%) and interferences in the infrared spectra. Because of the low concentrations encountered, chromatographic separation methods, such as thin-layer chromatography, were not pursued. An attempt was made to detect the presence of an organic vehicle in the pigment and preparation layers by using microscopical stains and fluorescence microscopy. Two fluorescent stains, fluorescein isothiocyanate and Rhodamine B, were used following the method of Wolbers and Landrey (1987). The first was dissolved in absolute ethanol (0.125 g in 50 ml). The second was dissolved in analytical-grade acetone at the same concentration. Samples were placed on microscope glass slides, and a drop of one of the stains was applied. After the solvent had evaporated and the stained sample dried, as indicated by a color change, a coverslip was applied. Mineral spirits was introduced under the coverslip by capillary action, and samples were studied by fluorescence microscopy. An aqueous, fluorescent stain, Fungi-Fluor, was used to detect the presence of fungal infestations in the paint layers.

Results

The cross sections generally revealed a rather simple sequence, with thin paint layers applied to a preparation layer on top of the original clay supporting surface. The clay support consisted of a heterogeneous aggregate of particles showing a wide range of shape and size. Voids, cracks, and other discontinuities were frequently observed in the support. Cleavage within the support was also quite common. Straw was identified in the clay underlayer of all fragments. The distribution of straw in the clay varied from separate individual fibers to coarse bundles. Paper samples observed in some fragments were processed straw fibers. Pigment layers were loose aggregates with often very poor adhesion.

White layers from the Mogao grottoes were composed primarily of calcite and talc with traces of calcium oxalates and quartz. Lead sulfate was also found. Black surface layers contained quartz, calcium oxalates, a trace of calcite, and possibly a trace of talc. Red layers were composed of hematite, quartz, calcite, and calcium oxalates. Black and red pigments could not be identified in all cases. Azurite, and possibly atacamite or paratacamite, was observed in blue layers. Greens at Bingling included botallackite, $CuCl_2 \cdot 3Cu(OH)_2 \cdot 3H_2O$, and possibly atacamite or paratacamite, $Cu_2(OH)_3Cl$, or a copper chloride hydroxide hydrate, $Cu_7Cl_4(OH)_{10} \cdot H_2O$. A gold-colored layer consisted of an alloy of gold and silver. Minium (red lead), Pb_3O_4, was also identified as a pigment at both the Mogao grottoes and the Bingling Temple grottoes, partially converted to reddish-brown or black plattnerite, PbO_2. Calcium carbonate (calcite) was observed in the preparation layer between the clay substrate and the pigment layers. It was also found as an additive to the clay support.

With two possible exceptions, no binding medium was detected by infrared spectroscopy in the samples from either the Mogao or Bingling Temple grottoes. The exceptions were the detection of trace amounts of organic material in a red surface layer from one fragment and in a black layer from another that could not, however, be attributed to a specific material. Attempts to isolate the organic material from the red layer for spectroscopic identification were unsuccessful. Similarly, no binding medium could be detected in the pigment layers using the microscopical staining method. This indicates that if there is a residual medium, it is present at a very low concentration. This is consistent with the observation of poor adhesion of pigments observed in the cross sections.

Calcium oxalates were detected in varying concentrations and were not restricted to any particular colors as they were identified in samples of white, black, red, green, and light blue paint. No appreciable concentration of oxalates was present in the clay layer under the pigmented surface layer, and no oxalates were detected in a fragment from a small building at the Mogao grottoes. Copper oxalate appeared to be present, along with botallackite, in the green samples from two fragments; however, the presence of calcium and copper oxalates was not confirmed by X-ray diffraction. The presence of calcium oxalates was usually determined from the infrared spectra. It is not possible to distinguish which hydrates of calcium oxalate were present by infrared spectroscopy.

Calcium oxalate exists in a number of hydration states, primarily weddellite ($CaC_2O_4 \cdot 2H_2O$), and whewellite ($CaC_2O_4 \cdot H_2O$) with other hydrated forms up to $CaC_2O_4 \cdot 3H_2O$. The copper oxalate may be the reaction product of a copper-containing pigment and oxalic acid.

The mechanism of incorporation of the oxalates into the paint layer has not been determined, but a number of possibilities exist (Moffatt, Adair, and Young 1985:234–38; Wiedemann and Bayer 1989:127–35). Calcium oxalates may have been present in the paint layer as an original constituent. They may have resulted from a treatment of the surface with oxalic acid, which subsequently reacted with calcite—present in the matrix—to form calcium oxalate. The origin of oxalates from the use of oxalic acid for cleaning and protective or aesthetic treatments has been the subject of speculation (Saiz-Jimenez 1989: 127–35; Moffatt, Adair, and Young 1985:234–38; Agrawal et al. 1987:447–52). Alternatively, the oxalates may be of microbiological origin. The formation of oxalates by microorganisms, such as lichens and fungi, is well documented (Saiz-Jimenez 1989:127–35). These oxalates, usually whewellite and weddellite, are produced by the reaction of calcium carbonate with the oxalic acid produced by lichens. No stained, fluorescent fungal hyphae were evident in any of the samples. Cellular debris of processed straw was observed in some of the paint layers, mainly pieces of parenchymatous cells, some whole cells, and segments of fibers. From the small amount of sample material investigated, no correlation could be shown between the presence of straw and the presence of calcium oxalate. Because many plants, including straw, produce quantities of oxalates, further study should be undertaken to determine if such a correlation exists.

Plattnerite (PbO_2) was observed in some samples. The mechanism of discoloration of red lead and its conversion to plattnerite has been discussed by West FitzHugh (1986:109–39) and by Petushkova and Lyalikova (1986:65–69) and was the subject of an unpublished investigation by Gettens (1935, 1936). It cannot be stated whether the transformation results from exposure to light, microbiological activity, or the presence of water or carbon dioxide.

Discussion

The typical structure of a wall painting at the Mogao or Bingling Temple grottoes begins with a supporting layer of clay, sometimes mixed with calcium carbonate, which was applied to the sandstone grotto wall to obtain a more even surface for working. A preparation layer consisting of clay and straw with calcium carbonate (e.g., chalk, whiting, lime white) was applied next, prior to the execution of the design surface itself. Materials, such as various clay minerals, insoluble salts, proteinaceous adhesives, and so on, react in moist or humid environments in ways that are damaging to painted surfaces. Clays form an integral part of the structure and fabrication of the wall paintings. Diurnal or seasonal variation in temperature and relative humidity within the grottoes can be expected to cause anisotropic expansion and contraction of clays with respect to the

sandstone wall and the paint (pigment) layers. It can be expected that this will result in a loss of adhesion within the clay layers and between the preparation layer and the pigments. The cross sections showed that cleavage and exfoliation are indeed occurring in these areas.

The colored pigments identified in this study were hematite, azurite, minium (red lead), and a number of copper compounds, including possible identifications of atacamite or paratacamite and a copper chloride hydroxide hydrate. The original black pigment was not positively identified but is most probably a bone black and not, for example, a charcoal black. The black mineral plattnerite, a conversion product of red lead, was also observed. The gold layer in one sample was an alloy of gold and silver. Because of the thin application of paint, it was frequently difficult to determine if white or translucent materials were intentional fillers or extenders of the paint or if they were part of the substrate or preparation layer. Such compounds included quartz, calcite, gypsum, talc, and possibly muscovite.

The absence of typical levels of binding medium found in paints in other cultural contexts, as well as the presence of calcium oxalates and the presence of plattnerite, suggest that the paintings have been subject to a complex process of deterioration that may include one or more microbiological processes. No evidence was found to allow a categorical statement of what precise environmental agent or agents were responsible for the occurrence of plattnerite or calcium oxalates.

Acknowledgments

The project summarized in this paper was undertaken at the Canadian Conservation Institute (CCI) in collaboration with Li Zuixiong of the Dunhuang Academy. The authors wish to thank the following for their advice and assistance in obtaining literature references: W. T. ("Tom") Chase, Technical Laboratory, Arthur M. Sackler Gallery, Freer Gallery of Art, Smithsonian Institution; Elisabeth West FitzHugh and John Winter, Freer Gallery of Art, Smithsonian Institution; the Center for Conservation and Technical Studies, Harvard University Art Museums; Maureen Clark, Library, Canadian Conservation Institute. The interest of Charles Gruchy, Director-General, Canadian Conservation Institute, who was instrumental in establishing a collaborative project between the CCI and the Dunhuang Academy, is gratefully acknowledged, as is the support of John Taylor and the late Kenneth Macleod.

Notes

1 A Leitz (Wetzlar) vertical fluorescence illuminator (after J. S. Ploem) was used on a Leitz Orthoplan microscope with a high-pressure mercury vapor lamp. It permits a selection of exciter filters that correspond to the ultraviolet, violet, blue, and green regions of the spectrum. Dichroic beam-splitting mirrors and matched barrier filters permit selection of the appropriate visible light fluorescence.

2 A Hitachi S-530 scanning electron microscope with a Tracor X-ray Microtrace Hypersense lithium-drifted silicon X-ray detector was used with a Tracor Northern TN-2010 spectrometer. Using this technique, chemical elements of an atomic number greater than or equal to 11 (sodium) present in the sample can be identified with a sensitivity of about 1%.

3 A Philips PW 1130 X-ray generator and a cobalt tube (with an iron beta filter to eliminate the cobalt K_β line) was used with a 114.6 mm diameter Debye-Scherrer X-ray diffraction camera and Gandolfi mechanism for small particulate samples and fragments. Samples were irradiated with cobalt K_α radiation, and patterns are recorded on CEA 25 film. Larger samples were analyzed with a Philips PW 1050/76 diffractometer (goniometer).

4 A Nicolet 5DX FTIR spectrometer was used in this study. For further information on the diamond anvil microsample cell, see Laver and Williams (1978:34–39).

Materials and Suppliers

Fluorescein isothiocyanate and **Rhodamine B** were obtained from Sigma Chemical Company, P.O. Box 14508, St. Louis, MO 63178.

Fungi-Fluor was obtained from Polysciences, Inc., 400-T Valley Road, Warrington, PA 18976-2590.

References

Agrawal, O. P., T. Singh, B. B. Kharbade, K. K. Jain, and G. P. Joshi
1987 Discolouration of Taj Mahal marble: A case study. In *Proceedings of the International Council of Museums (ICOM) Committee for Conservation, 8th Triennial Meeting, Sydney, 6–11 September 1987,* 447–52. Marina del Rey, Calif.: Getty Conservation Institute.

Delbourgo, S. R.
1980 Two Far Eastern artifacts examined by scientific methods. In *International Symposium on the Conservation and Restoration of Cultural Property: Conservation of Far Eastern art objects, 26–29 November 1979, Tokyo, Japan,* 173–79. Tokyo: Tokyo National Research Institute of Cultural Properties.

Gettens, R. J.
1935 Preliminary Report on Chinese Pigments (16 December). On file at the Conservation Department of the Fogg Museum of Art, Cambridge, Massachusetts.

1936 The Pigments of Central Asian Wall Paintings (July). On file at the Conservation Department of the Fogg Museum of Art, Cambridge, Massachusetts.

1938a Pigments in a wall painting from central China. *Technical Studies in the Field of the Fine Arts* 7(2):99–105.

1938b The materials in the wall paintings from Kizil in Chinese Turkestan. *Technical Studies in the Field of the Fine Arts* 6(4):281–94.

Grey, B.
1959 *Buddhist Cave Paintings at Tun-huang.* Chicago: University of Chicago Press.

Hsu Wei-yeh, Chou Kuo-hsia, and Li Yun-ho
1983 X-ray studies of the inorganic Tun-huang pigments. *Dunhuang Yanjiu* 1:187–97.

Laver, M. E., and R. S. Williams
1978 The use of a diamond cell microsampling device for infrared spectrophotometric analysis of art and archaeological materials. In *Journal of the International Institute for Conservation of Historic and Artistic Works (IIC)—Canadian Group* 3(2):34–39.

Moffatt, E. A., N. T. Adair, and G. S. Young
1985 The occurrence of oxalates on three Chinese wall paintings. In *Application of Science in Examination of Works of Art. Proceedings of the Seminar, 7–9 September 1983*. Ed. Pamela A. England and Lambertus van Zelst, 234–38. Boston: Museum of Fine Arts.

Petushkova, J. P., and N. N. Lyalikova
1986 Microbiological degradation of lead-containing pigments in mural paintings. *Studies in Conservation* 31(2):65–69.

Qi Yingtao
1984 Studies on conservation of the grotto temples and the mural paintings of ancient graves in China. In *International Symposium on the Conservation and Restoration of Cultural Property: Conservation and restoration of mural-paintings (1), 17–21 November 1983, Tokyo, Japan,* 19–29. Tokyo: Tokyo National Research Institute of Cultural Properties.

Saiz-Jimenez, C.
1989 Biogenic vs. anthropogenic oxalic acid in the environment. In *Oxalate films: Origin and Significance in the Conservation of Works of Art. Proceedings. Milan, 25–26 October 1989,* 207–14. Milan: Centro CNR Gino Bozza.

Warner, L.
1938 *Buddhist Wall Paintings: A Study of a Ninth-Century Grotto at Wan Fo Hsia.* Cambridge, Mass.: Harvard University Press.

West FitzHugh, E.
1986 Red lead and minium. In *Artists' Pigments: A Handbook of Their History and Characteristics,* 109–39. Cambridge: Cambridge University Press.

Wiedemann, H. G., and G. Bayer
1989 Formation of whewellite and weddelite by displacement reactions. In *Oxalate films: Origin and Significance in the Conservation of Works of Art. Proceedings. Milan, 25–26 October 1989,* 127–35. Milan: Centro CNR Gino Bozza.

Winter, J.
1984 Pigments in China: A preliminary bibliography. In *Preprints of the 7th Triennial Meeting of the ICOM Committee for Conservation, Copenhagen, 10–14 September 1984.* Ed. D. de Froment, 84.19.11. Paris: ICOM in association with the J. Paul Getty Trust.

Wolbers, R., and G. Landrey
1987 The use of direct reactive fluorescent dyes for the characterization of binding media in cross-sectional examinations. In *Preprints, American Institute for Conservation of Historic and Artistic Works (AIC), Vancouver, 20–24 May 1987,* 168–202. Washington, D.C.: AIC.

Color Measurement at the Mogao Grottoes

Michael R. Schilling, Li Jun, Li Tie Chao, Guo Hong, Li Zuixiong, and Duan Xu Xe

In 1989, a long-term project of monitoring, documentation, preservation, and training was initiated at the Mogao grottoes by the Getty Conservation Institute in collaboration with the State Bureau of Cultural Relics of the People's Republic of China and the Dunhuang Academy. An important aspect of the project was the study of the colors and appearance of the wall paintings and statues in the grottoes. Selected members of the staff of the Dunhuang Academy were instructed in the fundamentals of color measurement, the use of the instrumentation, normal operating procedures, and final data interpretation with the aim of establishing an ongoing program of color measurement at the Mogao grottoes (Schilling 1989). The following is a summary of the theory and practice of color measurement and its usefulness to the project.

Rationale for Color Documentation

Color documentation is an integral component of the project for a number of reasons. The primary purpose is to provide a stable record of the present appearance of the colors of the wall paintings at the inception of the project. Many factors can alter the appearance of the paintings' colors, such as physical aging or the methods used to preserve the paintings. To monitor the stability of the painted surfaces, it is imperative to have a record of the colors as they appear prior to treatment.

Color documentation is also important in laboratory experiments conducted at the Dunhuang Academy that are designed to study the darkening of red lead and other pigments when exposed to bright light and known relative humidity (Schilling 1989). The extent of color change can be quantified through the use of a numeric system of color expression.

Techniques for Documenting Color

Documentation of color can be accomplished by one of several methods. Color photography, the technique most frequently used in conservation, is an effective tool for quickly documenting the color and condition of objects. However, the value of the photographic record is severely limited

by the inaccuracy of color rendering and the impermanence of the dye layers and support.

A set of colored reference chips categorized by hue, value, and chroma (HVC) is the basis of the Munsell system of color notation. To describe an object's color with the Munsell system, the chip closest in color to the object is located and the HVC data on the chip noted. The quality of the color match strongly depends on lighting conditions and the color acuity of the observer (Billmeyer and Saltzman 1981).

Measuring devices, such as spectrophotometers and tristimulus colorimeters, offer another means of documenting color. These instruments provide a numeric expression of color that is based on mathematical conversions of tristimulus values. Numeric color records are inherently more accurate, precise, and stable than records obtained from other methods; therefore, they are preferred in conservation (Billmeyer and Saltzman 1981).

A Minolta Chroma Meter CR-121 was the instrument chosen to record the color data at the Mogao grottoes. The instrument is a portable, battery-operated, tristimulus colorimeter ideally suited for field projects and museum studies (Schilling 1993a, 1993b, 1993c). The measuring head has an aperture 3 mm in diameter and houses a built-in xenon flash. A small piece of Gore-Tex was applied to the end of the instrument to prevent damage to the wall paintings during measurement. The instrument was calibrated against a white ceramic tile prior to use.

CIELAB Color Notation

One of the most common numeric systems for expressing color or color difference is CIELAB notation, which utilizes the principle of opposing colors (Billmeyer and Saltzman 1981). Lightness is defined as L*, and hue is expressed in terms of a* and b*. Positive values of a* refer to red hues, and negative values to green hues. Similarly, yellows have positive b* values, and blues have negative values. Color data may be expressed graphically or in tabular form. Color charts, which are graphs of b* versus a*, or L* versus a*, are convenient for illustrating groups of color measurement data and for providing visual alternatives to data tables. Figure 1 illustrates some of the main features of the system.

Instrument Evaluation

An important component of any color monitoring program is the evaluation of the performance of the color-measuring device. In measurements of color difference, absolute accuracy is desirable but not critical. It is far more important that the measuring device be stable over the time period involved. Otherwise, any apparent color change would be indistinguishable from instrumental drift. Also, measurement reproducibility is also greatly affected by surface uniformity, which is significant, as the surfaces of wall paintings tend to be quite irregular.

Thus, the instrumental accuracy, stability, and reproducibility of the Minolta Chroma Meter CR-121 were evaluated to assess the effects of each on the measurement data. In measurements of British Ceramic

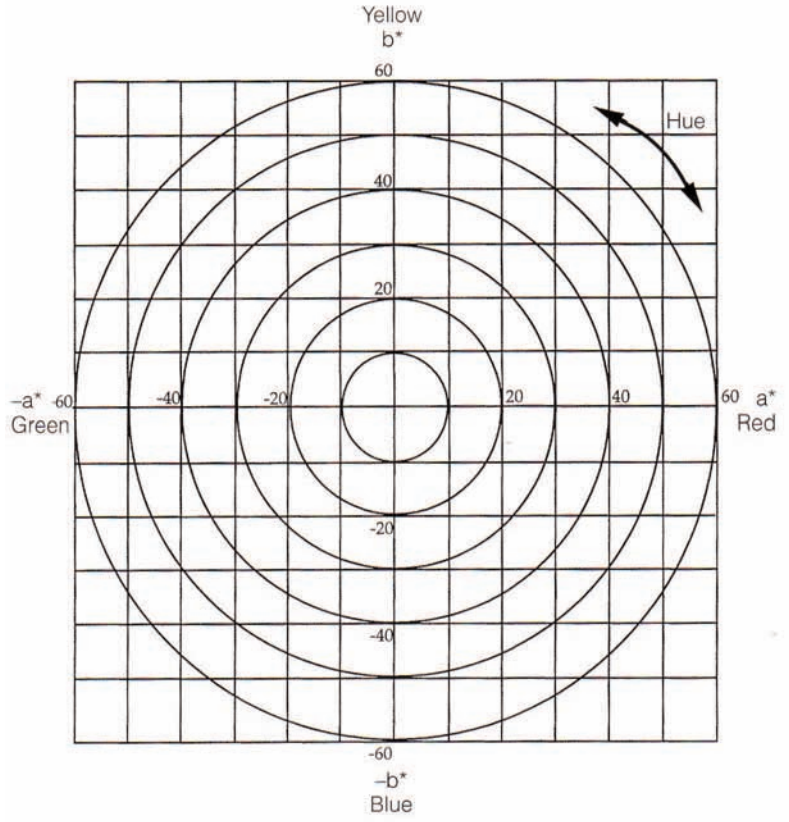

Figure 1
CIELAB color chart.

Research Association ceramic color standards (set CCS-II), the CR-121 consistently yielded results accurate to within one Munsell chip of the nominal value for the entire set of tiles. This performance, comparable to that of many human observers, is acceptable for most field conservation work. The stability of the CR-121, determined by periodic measurement of the CCS-II tiles, showed no pronounced long-term drift over the first two years of measurement. Reproducibility calculations were based on the measurement data from the wall paintings and sculpture (as discussed in the next section).

Measuring Technique

Color measurement of the wall paintings and statues at the Mogao grottoes involved the following procedure: Based on a thorough visual examination, measurement locations were selected to represent all of the colors present at each site. Measurements were made in six caves that were available for other scientific studies. As time permitted, additional measurements were made of both an outdoor painting above Cave 30 and the Pai Fang entryway (Table 1). Locations were recorded photographically and cross-referenced with site maps and floor plans for indexing purposes.

The painted surfaces were prepared for measurement by light dusting with a squirrel-hair brush, under a gentle stream of air produced by a rubber-bulb syringe. This procedure removed any surface dust that may have settled on the paintings that could affect the quality and reproducibility of the data.

Table 1 Measurement totals

Cave no.	Size	Open/closed to public	No. of measurements
35	large	closed	270
29	large	open	279
335	medium	closed	252
323	medium	open	342
232	small	closed	223
236	small	open	225
		Subtotal	1,591
		Outdoor mural above Cave 30	45
		Pai Fang entryway	63
		Total	1,699
Measurement totals by dynasty:	Tang:	1,168	
	Song:	261	
	Qing:	270	

Because of the inhomogeneity and irregularity of the painted surfaces and the difficulty in precisely locating the measuring head at each desired point, single measurements at each location could yield misleading results. Accordingly, three locations were selected within each colored area, each of which was measured three times. Measurement reproducibility was calculated from the three measurements at each area.

Results and Discussion

Color measurement data were entered into a database for archival purposes and for subsequent statistical and graphical interpretation. Tabulated data were sorted by cave, dynasty, and color. Because little or no information can be obtained from the measurement data of neutrals (black or white), these measurement data were not evaluated.

As mentioned, replicate measurements of each colored area were made in order to establish the limits of perceptible color change that can be measured by the CR-121. Standard deviations were calculated for the triplicate measurements for each of the three chromaticity variables and averaged over the entire set of 1,699 measurements. The one-sigma results are ± 0.3 Y, ± 0.001 x,y.

CIELAB charts of the data acquired at each site illustrate the range of palette found in the paintings and statues and are useful for comparing colors from different locations. Figures 2–4 show marked similarity of the palettes between pairs of matched caves (note, for example, the consistent overlay of the data for the small caves). The numbers illustrate that the pairs of caves share similar color schemes (besides the similarities in physical dimensions and dynastic period).

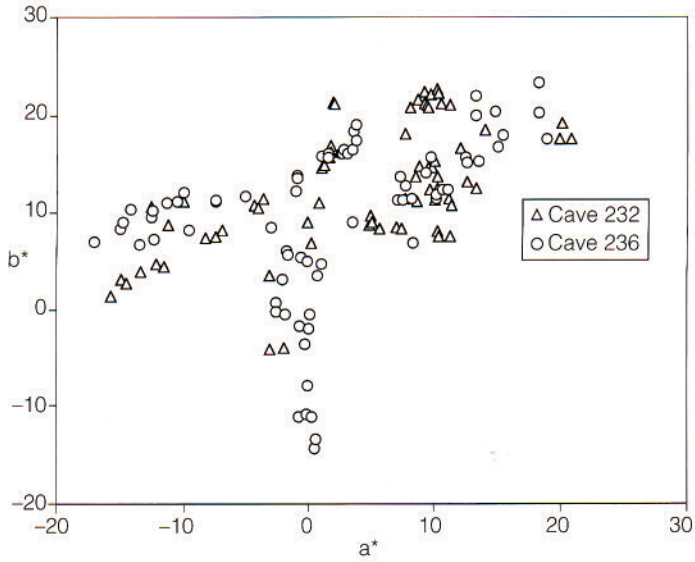

Figure 2
CIELAB data from small caves in the Mogao grottoes. Cave 236 is open to the public; Cave 232 is closed to the public.

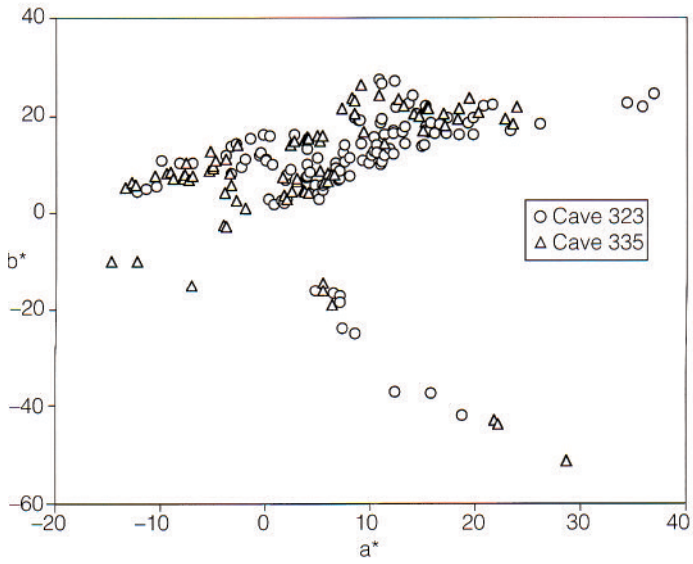

Figure 3
CIELAB data from medium caves in the Mogao grottoes. Cave 323 is open to the public; Cave 335 is closed to the public.

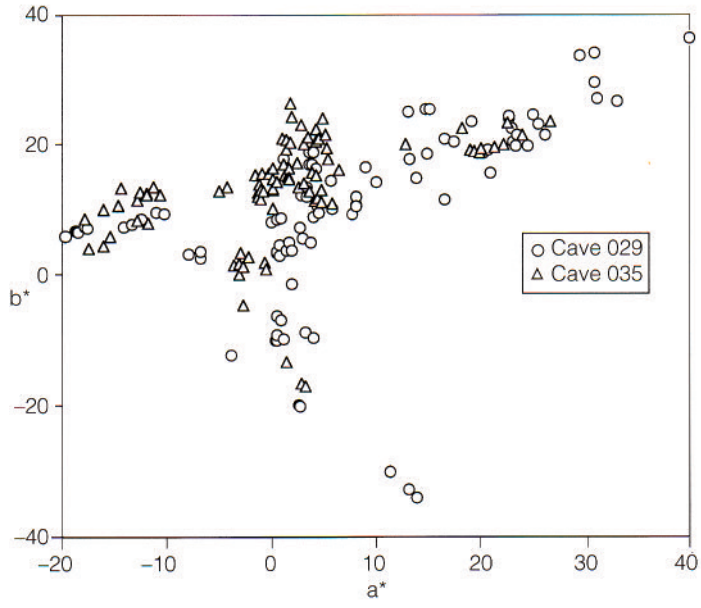

Figure 4
CIELAB data from large caves in the Mogao grottoes. Cave 29 is open to the public; Cave 35 is closed to the public.

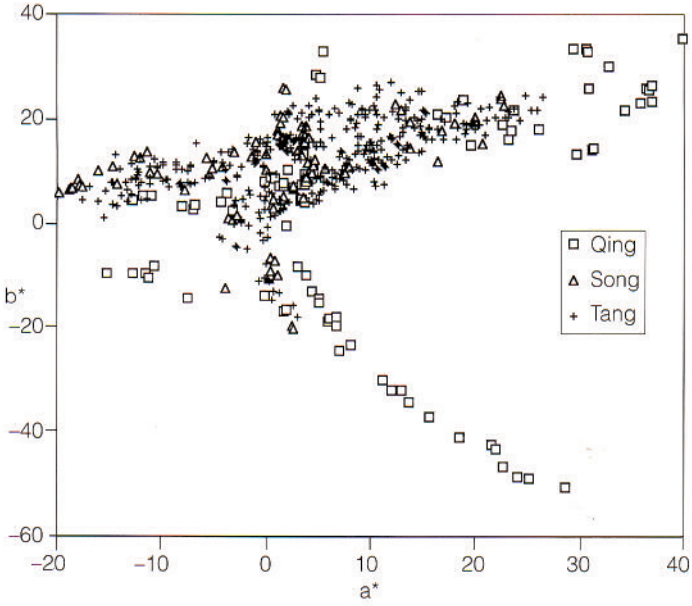

Figure 5
CIELAB data from the Mogao grottoes, sorted by dynasty.

The colors used in the Tang- and Song-dynasty paintings exhibit very low saturation, as evidenced by the closeness of the measurement data to the coordinates of the white-light source in Figure 5. On the other hand, Qing-dynasty paintings have significantly higher levels of saturation, presumably because the painted surfaces are cleaner and less weathered than earlier paintings. Because of this, Qing paintings can be readily distinguished from paintings made in other dynastic periods solely on the basis of color data. Although little distinction can be made between Tang and Song paintings, a complete statistical analysis of a large number of Tang and Song paintings may reveal certain trends that would permit differentiation between paintings from these two dynasties.

Conclusions

The utility of the color monitoring data lies in the establishment of a permanent record of the colors of the cave paintings and statues at the Mogao grottoes as they presently appear. From these data, a master color record for each cave and statue can be compiled. Ultimately, the color record will be a benchmark against which the success of any future preservation efforts will be judged.

Acknowledgments

The authors wish to thank Neville Agnew, associate director, programs, the Getty Conservation Institute, for direction during this project. Max Saltzman, expert on color technology, provided invaluable information and insight on all aspects of this work.

References

Billmeyer, F., Jr., and M. Saltzman

1981 *Principles of Color Technology.* 2d ed. New York: Wiley.

Schilling, Michael

1989 Mogao grottoes project. Report. Marina del Rey, Calif.: Getty Conservation Institute.

1993a Color measurement of the wall paintings in the tomb of Nefertari. In *Preprints of the ICOM Committee for Conservation 10th Triennial Meeting, Washington, D.C., 22–27 August 1993,* ed. Janet Bridgland. Paris: International Council of Museums (ICOM).

1993b The color measurement program in the tomb of Nefertari. In *Art and Eternity: The Nefertari Wall Paintings Conservation Project, 1986-1992,* ed. Miguel Angel Corzo and Mahasti Afshar. Marina del Rey, Calif.: Getty Conservation Institute.

1993c Yungang grottoes project. Report. Marina del Rey, Calif.: Getty Conservation Institute.